IOP Publishing

Journal of Physics: Condensed Matter

J. Phys.: Condens. Matter **27** (2015) 255002 (6pp)

doi:10.1088/0953-8984/27/25/255002

Negative tunneling magneto-resistance in quantum wires with strong spin–orbit coupling

Seungju Han[1], Llorenç Serra[2] and Mahn-Soo Choi[1]

[1] Department of Physics, Korea University, Seoul 136-701, Korea
[2] IFISC (CSIC-UIB) and Department of Physics, University of the Balearic Islands E-07122 Palma de Mallorca, Spain

E-mail: choims@korea.ac.kr

Received 28 January 2015, revised 31 March 2015
Accepted for publication 2 April 2015
Published 28 May 2015

Abstract

We consider a two-dimensional magnetic tunnel junction of the FM/I/QW(FM+SO)/I/N structure, where FM, I and QW(FM+SO) stand for a ferromagnet, an insulator and a quantum wire with both magnetic ordering and Rashba spin–orbit (SOC), respectively. The tunneling magneto-resistance (TMR) exhibits strong anisotropy and switches sign as the polarization direction varies relative to the quantum-wire axis, due to interplay among the one-dimensionality, the magnetic ordering, and the strong SOC of the quantum wire.

Keywords: tunneling magneto-resistance, quantum wire, LAO/STO

(Some figures may appear in colour only in the online journal)

1. Introduction

The magnetic tunneling junction (MTJ) consisting of two ferromagnetic electrodes (FM) separated by a thin insulating barrier (I) is a prototype structure in the rapidly developing field of spintronics [1]. The tunneling magneto-resistance (TMR), depending on the relative magnetic polarization of the two ferromagnets, is a key issue not only for the spintronic applications but also for the study of fundamental magnetic properties [2, 3]. Due to the spin selection rule the TMR, if any, is typically positive. Two exceptional cases have been known. One involves magnetic impurities in the tunnel barriers and is not surprising. The other (more important) case is associated with the resonant tunneling and spin-dependent interfacial phase shift in double-barrier FM/I/N/I/FM structures, where N represents a non-magnetic normal metal [4–8].

In this work we explore another non-trivial example of negative TMR in a *two-dimensional* (2D) double-barrier MTJ of the FM/I/QW(FM+SO)/I/N structure (see figure 1(*a*)), where QW(FM+SO) stands for a quantum wire (QW) with both magnetic ordering and Rashba spin–orbit coupling (SOC). Our MTJ structure should be distinguished from more common 1D MTJs of the FM/I/QW/I/FM structure such as in [5], where the QW is non-magnetic and the junction interface is perpendicular to the quantum-wire axis. In our case, the QW itself has a magnetic ordering and the junction interface is parallel to its axis. Thus, transport occurs across, not along the quantum wire. We find that the TMR exhibits strong anisotropy and even changes sign as the polarization direction of the ferromagnets varies relative to the quantum-wire axis. This sign-switching anisotropic TMR is attributed to the interplay among the one-dimensionality, the magnetic ordering, and the strong SOC of the QW. It is interesting to recall that anisotropic TMR was previously studied in the FM/I/FM structure where the insulating barrier (not the ferromagnets) had SOC (see [9] and references therein), but the TMR remained positive without switching its sign.

Our MTJ structure is peculiar in that the nanoscale quantum wire has both strong SOC and magnetic ordering. One important motivation for our MTJ structure is (but is not limited to) the recent experiment [10] on the transition metal oxide interface between $LaAlO_3$ (LAO) and $SrTiO_3$ (STO) (see figure 1(*b*)), where the measured TMR is strongly anisotropic and switches sign as the magnetization direction varies in the interface plane. Since the LAO/STO interface

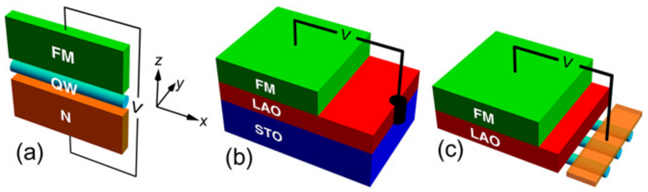

Figure 1. (*a*) A double-barrier MTJ of the FM/I/QW(FM+SO)/I/FM structure. (*b*) A setup to measure the TMR between the ferromagnetic top electrode and the LAO/STO interface. (*c*) A simplified model of (*b*).

was demonstrated a decade ago [11] to be metallic even though both LAO and STO are typical band insulators, it has attracted ever-growing interest by exhibiting superconductivity [12], ferromagnetism [13] and even coexistence of both effects [14, 15]. Despite a number of experimental studies of the system, the origins of magnetic ordering and superconductivity remain controversial [16, 17] and further studies are imperative. The sign-switching anisotropic TMR [10] adds a fresh intriguing question concerning the magnetic properties of the LAO/STO interface. Our results below suggest one possible explanation for it in terms of our MTJ model mentioned above. Our present purpose is not modeling of any specific device but suggesting a scenario of physical effects.

Indeed, a recent experiment [18] suggests that the electric conduction in the LAO/STO interface (figure 1(*b*)) occurs mainly along the narrow paths associated with the twin boundaries in the STO crystal. At the lowest approximation, one can ignore the direct coupling between the narrow conducting paths, which are regarded as QWs; see figure 1(*c*). As the resistance occurs dominantly at the tunnel junction between the ferromagnetic top electrode and the quantum wire, one can ignore the resistance along the QWs and the MTJ structures in figures 1(*a*) and (*c*) are essentially the same.

Recently, isolated quantum wires with true one-dimensional character have also been formed artificially on the LAO/STO interface by alternating two LAO stripes of different thicknesses, and significantly enhanced ballistic quantum transport along them has been demonstrated [19]. These quantum wires naturally have both strong SOC and magnetic ordering inherited from the LAO/STO interface. Once the ferromagnetic top electrode is fabricated, such a device will be an idealistic realization of our MTJ structure.

The rest of the paper is organized as follows. In section 2, the model Hamiltonian is defined and the basis states to compose the scattering states are specified. In section 3, the numerically exact results of the TMR ratio are reported. It is demonstrated that the TMR ratio exhibits a strong anisotropy and reverses sign as the magnetic polarization direction varies. Remarkably, this sign reversal can be tuned with an electric gate. Sections 4 and 5 are devoted to explaining analytically and qualitatively the sign-switching anisotropic behavior of the TMR ratio found in section 3. First, section 4 discusses the characteristics of the single interface between the ferromagnetic top electrode and the quantum wire. Then, the full double-barrier structure is discussed in section 5. Finally, section 6 concludes the paper.

2. Model

The MTJ is described by the Hamiltonian

$$H = \frac{p_x^2 + p_z^2}{2m} + U(z) - \frac{\alpha(z)}{\hbar} p_x \sigma_y - \mathbf{\Delta}(z) \cdot \boldsymbol{\sigma} , \qquad (1)$$

where σ_x, σ_y, and σ_z are the Pauli matrices. We have chosen the x-axis along the quantum-wire axis and the z-axis perpendicular to the junction interface (figure 1(*a*)). The direction of the effective field ('Rashba field') due to the Rashba SOC is along the y-axis, as it arises from the structural inversion symmetry breaking and should be perpendicular to both x- and z-axis. The Rashba SOC is present only on the QW ($0 < z < d$):

$$\alpha(z) = \begin{cases} \alpha_0 & (0 < z < d) \\ 0 & (\text{otherwise}) \end{cases} \qquad (2)$$

where $d \sim 1$ nm represents the diameter of the QW or the thickness of the LAO/STO interface. The Zeeman field $\mathbf{\Delta}(z)$ is due to the ferromagnetism on the top electrode and the QW and is modeled as a vector in the xy plane

$$\mathbf{\Delta}(z) = \begin{cases} \Delta_1(-\sin\phi, \cos\phi, 0) & (z > d)\ , \\ \Delta_2(-\sin\phi, \cos\phi, 0) & (0 < z < d)\ , \\ 0 & (z < 0), \end{cases} \qquad (3)$$

where the angle ϕ ($0 < \phi < \pi$) is measured from the y-axis (Rashba field direction). We assume that $\Delta_1 > 0$ and that $\Delta_2 > 0$ and $\Delta_2 < 0$ for the parallel (P) and anti-parallel (AP) configuration of the magnetic polarization directions, respectively. The chemical potentials (carrier densities) in different regions are described by potential steps and the thin insulating barriers by δ-potentials, giving the potential profile $U(z)$ of the form

$$U(z) = U_1\theta(z-d) + U_2[\Theta(z-d) - \Theta(z)] + a_b U_b \delta(z-d) + a_b' U_b' \delta(z)\ . \qquad (4)$$

U_b is responsible for the insulating layer of LAO, a_b is the effective width of the barrier ($a_b \sim 1$–5 nm), U_b' is responsible for the junction between the QW and the normal electrode and a_b' is its effective length scale. Experimentally, U_1 and U_2 correspond to chemical potentials in the corresponding regions. For a typical LAO/STO interface [16, 20–22], the Fermi energy $E_F \sim 40$ meV, $\alpha_0 \sim \hbar v_F^0/8$ with $v_F^0 \equiv \sqrt{2E_F/m}$, $\Delta_2 \sim E_F/16$, and $d \sim 1$ nm.

The model in equation (1) has been constructed mainly focusing on the device of the form in figure 1(*a*) and hence ignoring the motion in the y-direction. However, it is still relevant for more realistic devices like figure 1(*c*). In such a case, one has only to integrate over the transverse momentum k_y in the regions $z > d$ and $z < 0$, without affecting the qualitative features of our findings to be discussed below. The results are also insensitive to the width of the QW in the y-direction as long as it is small compared with the thickness in the z-direction and the Fermi wavelength.

The momentum in the x-direction is preserved over a tunneling process; here the junction (QW) is assumed to be infinitely wide (long). We thus seek a wave function of the form

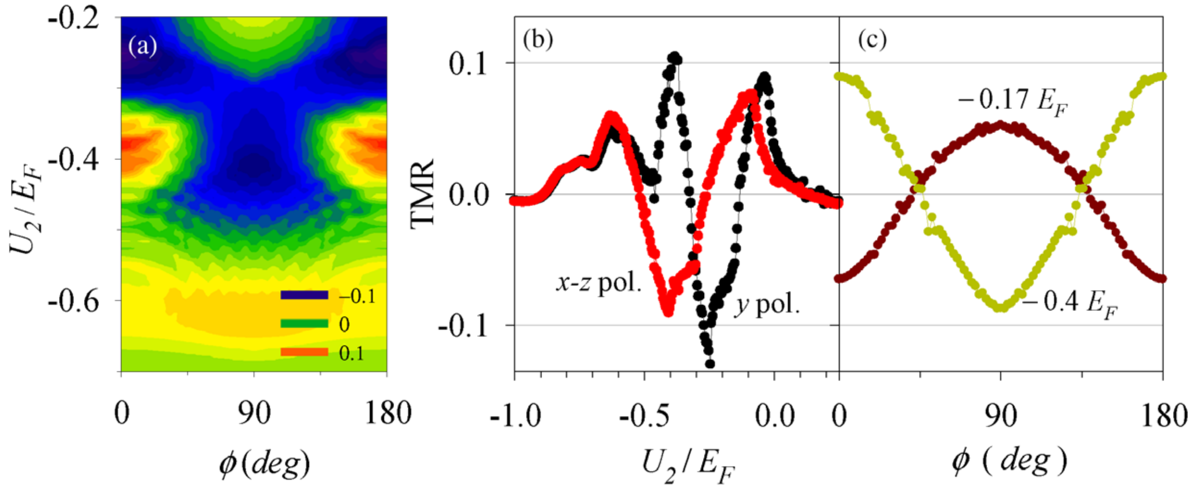

Figure 2. (*a*) Numerical results of the TMR as a function of U_2 and ϕ for $d = 4.5/k_F^0$ ($k_F^0 \equiv \sqrt{2mE_F/\hbar^2}$), $\alpha_0 = \hbar v_F^0/8\sqrt{2}$, $\Delta_1 = E_F/8$, $\Delta_2 = E_F/16$ and $U_1 = E_F/4$. (*b*) Cuts along $\phi = 0$ (black dots, y polarization) and $\phi = \pi/2$ (red-gray dots, x–z polarization). (*c*) Cuts along ϕ for the indicated fixed values of $U_2 = -0.17E_F$ and $U_2 = -0.40E_F$.

$\Psi(x, z) = e^{iqx}\psi(z)$, where $\psi(z)$ satisfies the 1D Schrödinger equation $H_z\psi(z) = \left(E - \hbar^2q^2/2m\right)\psi(z)$. The 1D effective Hamiltonian H_z is given by

$$H_z = \begin{bmatrix} 1 & 0 \\ 0 & 1 \end{bmatrix} \left(-\frac{\hbar^2}{2m}\frac{d^2}{dz^2} + U_1 \right) - \Delta_1 \begin{bmatrix} 1 & 0 \\ 0 & -1 \end{bmatrix} \tag{5}$$

in the region $z > d$, by

$$H_z = \begin{bmatrix} 1 & 0 \\ 0 & 1 \end{bmatrix} \left(-\frac{\hbar^2}{2m}\frac{d^2}{dz^2} + U_2 \right) - \begin{bmatrix} \alpha_0 q\cos\phi + \Delta_2 & -i\alpha_0 q\sin\phi \\ i\alpha_0 q\sin\phi & -(\alpha_0 q\cos\phi + \Delta_2) \end{bmatrix} \tag{6}$$

in the region $0 < z < d$, and by

$$H_z = \begin{bmatrix} 1 & 0 \\ 0 & 1 \end{bmatrix} \left(-\frac{\hbar^2}{2m}\frac{d^2}{dz^2} \right) \tag{7}$$

in the region $z < 0$. Here the spin part of H_z has been represented in the eigenbasis $\{|\chi_\uparrow\rangle, |\chi_\downarrow\rangle\}$ of $\sigma_y\cos\phi - \sigma_x\sin\phi$ corresponding to the Zeeman field of the ferromagnetic top electrode (region $z > d$). In the region $z > d$, the plane waves of the form

$$|\chi_{\uparrow/\downarrow}\rangle e^{ik_{\uparrow/\downarrow}z}, \quad |\chi_{\uparrow/\downarrow}\rangle e^{-ik_{\uparrow/\downarrow}z} \tag{8}$$

with $k_{\uparrow/\downarrow} \equiv \sqrt{2m(E - U_1 \pm \Delta_1)/\hbar^2 - q^2}$ compose the wave function $\psi(z)$. In the region $0 < z < d$, $\psi(z)$ is a linear combination of the plane waves of the form

$$|\chi_\pm\rangle e^{ik_\pm z}, \quad |\chi_\pm\rangle e^{-ik_\pm z} \tag{9}$$

where $k_\pm \equiv \sqrt{2m(E - U_2 \pm \Delta_2)/\hbar^2 - q^2}$ and

$$|\chi_+\rangle = \cos(\theta/2)|\chi_\uparrow\rangle + i\sin(\theta/2)|\chi_\downarrow\rangle \tag{10a}$$

$$|\chi_-\rangle = i\sin(\theta/2)|\chi_\uparrow\rangle + \cos(\theta/2)|\chi_\downarrow\rangle. \tag{10b}$$

Here the angle θ $(0 < \theta < \pi)$ switches between θ_P and θ_{AP} upon the P $(\theta = \theta_P)$ and AP $(\theta = \theta_{AP})$ configuration, which are defined by

$$\tan\theta_{P/AP} = \frac{\alpha_0 q\sin\phi}{\alpha_0 q\cos\phi \pm \Delta_2}. \tag{11}$$

Imposing proper matching conditions over δ-potentials at $z = 0$ and d, we determine (both with numerically exact method and with analytically approximate method) the scattering wave function $\psi(z)$ and calculate the TMR ratio, $\text{TMR} \equiv 1 - R_P/R_{AP}$, where $R_{P/AP}$ is the resistance for the P/AP polarization.

The analytical solution of the full double-barrier problem with proper matching conditions should be straightforward in principle. However, in practice it leads to a lengthy expression of the transmission even for a given direction of the incidence momentum, and it should additionally be integrated over the incidence angle. As it does not provide a clear physical insight, below we discuss qualitative features of the analytical approach, as well as the numerical exact results.

3. Exact results

Figure 2 shows the numerically exact results of the TMR as a function of U_2 and ϕ for a typical set of parameters consistent with the LAO/STO interface [16, 20–22]. The numerical method involves the integration of the transmission probabilities over the angle of the incident wave. The algorithm has been devised in such a way as to ensure a sufficient precision for the angular integrals. The details of the numerical method are described in a previous work by one of the authors [23].

It is shown in figure 2 that the TMR can be negative, as much as −10%. Further, it reveals two additional interesting features: first, the TMR depends rather strongly on U_2 (figure 2(*b*)). Experimentally, U_2 corresponds to the backgate voltage and controls the carrier density on the QW (or the LAO/STO interface). In the recent experiment [10], on the other hand, the TMR did not depend much on the gate voltage. However, the actual gate capacitance was not known and it is not clear how large is the actual energy range covered by the gate voltage variation. The gate voltage dependence needs to be tested further. Moreover, in real samples (even if there are twin boundaries) the electric conduction is not completely confined to the narrow paths.

A second remarkable thing about figure 2 is the change of the ϕ dependence from a $\cos(\phi/2)$ to a $-\cos(\phi/2)$ behavior by tuning the value of U_2 (figure 2(*c*)). This is seen as a reversed change of sign of the TMR when going from $\phi = 0$ to $\phi = \pi/2$; from positive to negative for $U_2 = -0.4E_F$, and reversed for $U_2 = -0.17E_F$.

As we discuss below, both features of the exact results can be understood qualitatively by means of an analytical (but approximate) method.

4. Qualitative features of single-barrier tunneling

We first examine the transmission over the *first barrier* at $z = d$. Before going further, recall the transmission problem of a *spinless particle* with energy E over a potential barrier U_b, $U(z) = U_1\Theta(-z) + U_2\Theta(z) + a_bU_b\delta(z)$. The transmission amplitude t is given by

$$t(q_b; k_1, k_2) = \frac{\sqrt{k_1k_2}}{(k_1 + k_2)/2 + \mathrm{i}q_b}\ , \tag{12}$$

where $k_j \equiv \sqrt{2m(E - U_j)/\hbar^2}$ and $q_b \equiv ma_bU_b/\hbar^2$. When the barrier is sufficiently high ($U_b \gg E$), it can be approximated as

$$t(q_b; k_1, k_2) \approx \frac{\sqrt{k_1k_2}}{\mathrm{i}q_b}\ . \tag{13}$$

Consider now a scattering state $\psi_\pm(z)$ of the form

$$\psi_\pm(z) = \begin{cases} \sum\limits_{s=\uparrow,\downarrow} \left(A_s|\chi_s\rangle \mathrm{e}^{-\mathrm{i}k_sz} + B_s|\chi_s\rangle\mathrm{e}^{\mathrm{i}k_sz}\right) & (z > d) \\ C_\pm|\chi_\pm\rangle\mathrm{e}^{-\mathrm{i}k_\pm z} & (z < d) \end{cases} \tag{14}$$

Here we have imposed a boundary condition such that in the region $z < d$ there is only one propagating spin channel $|\chi_\mu\rangle$ of fixed $\mu = \pm$. On the one hand, the coefficients A_s and C_μ are related through the transmission coefficients $t_{\mu s}$ by $C_\mu = \sum_s t_{\mu s}A_s$. On the other hand, the matching conditions over the δ-barrier are equivalent to those on the wave function of the form

$$\eta_{\mu s}(z) = \begin{cases} A_s\mathrm{e}^{-\mathrm{i}k_sz} + B_s\mathrm{e}^{\mathrm{i}k_sz} & (z > d) \\ C_\mu\langle\chi_s|\chi_\mu\rangle\mathrm{e}^{-\mathrm{i}k_\mu z} & (z < d) \end{cases} \tag{15}$$

imposed separately for each component $s =\uparrow, \downarrow$. This implies by equation (12) that $C_\mu\langle\chi_s|\chi_\mu\rangle = A_st(q_b; k_\mu, k_s)$. Combining these two relations leads to

$$\begin{bmatrix} 1 & 0 \\ 0 & 1 \end{bmatrix} = \begin{bmatrix} t_{+\uparrow} & t_{+\downarrow} \\ t_{-\uparrow} & t_{-\downarrow} \end{bmatrix} \begin{bmatrix} \frac{\langle\chi_\uparrow|\chi_+\rangle}{t(q_b;k_+,k_\uparrow)} & \frac{\langle\chi_\uparrow|\chi_-\rangle}{t(q_b;k_-,k_\uparrow)} \\ \frac{\langle\chi_\downarrow|\chi_+\rangle}{t(q_b;k_+,k_\downarrow)} & \frac{\langle\chi_\downarrow|\chi_-\rangle}{t(q_b;k_-,k_\downarrow)} \end{bmatrix} \tag{16}$$

Using the approximation (13), the matrix on the right hand side of (16) is factorized as

$$\begin{aligned} \begin{bmatrix} t_{+\uparrow} & t_{+\downarrow} \\ t_{-\uparrow} & t_{-\downarrow} \end{bmatrix} &\approx \mathrm{i} \begin{bmatrix} \sqrt{k_+/q_b} & 0 \\ 0 & \sqrt{k_-/q_b} \end{bmatrix} \\ &\times \begin{bmatrix} \langle\chi_+|\chi_\uparrow\rangle & \langle\chi_+|\chi_\downarrow\rangle \\ \langle\chi_-|\chi_\uparrow\rangle & \langle\chi_-|\chi_\downarrow\rangle \end{bmatrix} \\ &\times \begin{bmatrix} \sqrt{k_\uparrow/q_b} & 0 \\ 0 & \sqrt{k_\downarrow/q_b} \end{bmatrix} \end{aligned} \tag{17}$$

The transmission probabilities $T_\mu(q) \equiv \sum_s |t_{\mu s}|^2$ for the channels $\mu = \pm$ are given by

$$T_\pm(q) \approx \frac{k_\uparrow + k_\downarrow}{2q_b}\left[\frac{k_\pm}{q_b} \pm \frac{4m\Delta_1}{\hbar^2(k_\uparrow + k_\downarrow)^2}\cos\theta\right] \tag{18}$$

where the q-dependence of $k_{\uparrow/\downarrow}$, $k_\pm$ and θ is implied. The expressions (18) for the transmission probabilities between a ferromagnet and another ferromagnet with strong Rashba SOC is one of our main results.

5. Qualitative features of the double-barrier structure

Now we investigate the full double-barrier structure for all possible values of q. For high tunnel barriers, the wave number $k_\pm$ in the central region ($0 < z < d$) is quantized to $k_n \approx n\pi/d$ ($n = 1, 2, \cdots$) and the wave function takes the form $\Psi(x, z) = |\chi_\pm(q^\nu_{n,\pm})\rangle \sin(k_nz)\mathrm{e}^{\mathrm{i}q^\nu_{n,\pm}x}$. For each k_n and a given energy E, the allowed values $q^\nu_{n,\pm}$ ($\nu =\lessgtr$) is determined by the dispersion relation

$$\begin{aligned} E = \frac{\hbar^2}{2m}\left[k_n^2 + (q^\nu_\pm)^2\right] + U_2 \\ \mp \sqrt{\left(\alpha_0q^\nu_{n,\pm}\right)^2 + 2\left(\alpha_0q^\nu_{n,\pm}\right)\Delta_2\cos\phi + \Delta_2^2}\,. \end{aligned} \tag{19}$$

Due to narrow confinement ($d \sim 1$ nm) and strong SOC ($\alpha q \simeq E/8$), typically only one $k_n^\pm$ is allowed for each $\pm$. Hereafter we thus drop the subscript n: $k \equiv k_n$, $q^\nu_\pm \equiv q^\nu_{n,\pm}$ and $|\chi^\nu_\pm\rangle \equiv |\chi_\pm(q^\nu_{n,\pm})\rangle$. The total transmission probability is given by $T = \sum_{\mu=\pm}\left[T_\mu(q^>_\mu) + T_\mu(q^<_\mu)\right]$.

For $\phi = \pi/2$, the Zeeman field is perpendicular to the Rashba field and the dispersion relation is particularly simple. Especially, one has $q^>_\pm = -q^<_\pm \equiv q_\pm$, $q_+ > q_-$, $\cos\theta_P(q_\pm) > 0$, $\cos\theta_{AP}(q_\pm) < 0$, and $T = 2\left[T_+(q_+) + T_-(q_-)\right]$. When both $q_\pm$ contribute to the transport (figure 3(*a*)),

$$\begin{aligned} \mathrm{TMR} \propto &\frac{\cos\theta_P(q_+) - \cos\theta_{AP}(q_+)}{k_\uparrow(q_+) + k_\downarrow(q_+)} \\ &- \frac{\cos\theta_P(q_-) - \cos\theta_{AP}(q_-)}{k_\uparrow(q_-) + k_\downarrow(q_-)} \end{aligned} \tag{20}$$

The q_+ (q_-) channel contributes a positive (negative) TMR. As $q_+ > q_-$, $k_\uparrow(q_+) + k_\downarrow(q_+) < k_\uparrow(q_-) + k_\downarrow(q_-)$ and the positive contribution from q_+-channel dominates. When q_+-channel is not allowed (figure 3(*b*)), $T_-(q_-)$ from the q_- channel is the sole contribution and the TMR becomes negative.

For $\phi = 0$ ($\phi = \pi$), $\theta_P(q^\gtrless_\pm) = \theta_{AP}(q^\gtrless_\pm) = 0$ and the total transmission reads as (equation (18) with $k_\pm = k$)

$$T = \frac{k}{q_b^2}\left[k_\downarrow(q^>_-) + k_\uparrow(q^<_-) + k_\downarrow(q^<_+) + k_\uparrow(q^>_+)\right]. \tag{21}$$

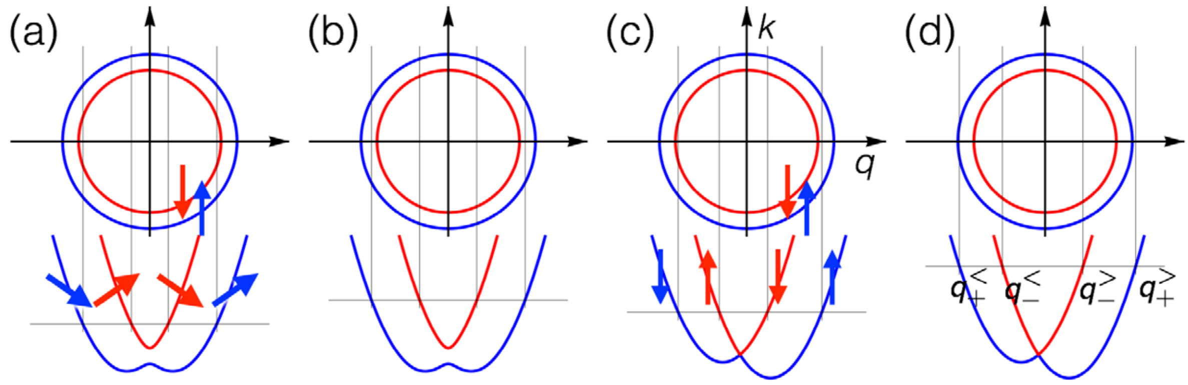

Figure 3. The spin-split Fermi circles in the ferromagnetic top electrode (top) and the dispersion relation in the QW (bottom) for $\phi = \pi/2$ ((*a*) and (*b*)) and for $\phi = 0$ ((*c*) and (*d*)). The thin horizontal lines indicate the Fermi levels *relative to the band bottoms* and the short arrows depict the spin quantization directions. In (*a*) and (*c*) all transverse modes at the Fermi level on the QW contribute to the transport, whereas the two outer modes in (*b*) and the $q_+^>$-mode in (*d*) do not.

Note that $q_+^> > -q_+^< > -q_-^< > q_-^> > 0$ in the P polarization configuration (figures 3(*c*) and (*d*)). The TMR is then given by

$$\begin{aligned} \mathrm{TMR} \propto & [k_\uparrow(q_+^>) - k_\downarrow(q_+^>)] - [k_\uparrow(q_+^<) - k_\downarrow(q_+^<)] \\ & + [k_\uparrow(q_-^<) - k_\downarrow(q_-^<)] - [k_\uparrow(q_-^>) - k_\downarrow(q_-^>)] \end{aligned} \tag{22}$$

where the terms have been arranged in decreasing order (all values within square brackets are positive) and all $q_\pm^{\gtrless}$ have been defined for the P polarization configuration. As U_2 (the chemical potential in the central region) varies, the $q_+^>$ channel may become disallowed (figure 3(*d*)). In such a case, there are more negative contributions to the TMR. As U_2 varies further, the $q_+^<$ channel is also disallowed, and the TMR becomes positive again. As U_2 varies even further, the $q_-^<$ channel stops contributing to the transport and the TMR becomes negative once more.

Putting all together, with $U_2 \to -\infty$, TMR is positive both at $\phi = 0$ and $\phi = \pi/2$. As U_2 moves up, the $q_+^>$-mode at $\phi = \pi/2$ gets disallowed first at $U_2 \approx -0.6E_\mathrm{F}$; the TMR($\phi = \pi/2$) becomes negative but TMR(0) remains positive. At $U_2 \approx -0.5E_\mathrm{F}$, the $q_+^>$ mode at $\phi = 0, \pi$ gets disallowed and both TMR($\pi/2$) and TMR(0) become negative. But quite soon at $U_2 \approx -0.45E_\mathrm{F}$, the $q_+^<$ mode gets disallowed and TMR(0) quickly becomes positive again. Therefore, until $U_2 \approx -0.2E_\mathrm{F}$, where both spin channels get disallowed, TMR($\pi/2$) and TMR(0) remain negative and positive, respectively. As a function of ϕ, the TMR is expected to behave like $\cos(\phi/2)$. This is consistent with figures 2(*b*) and (*c*) for $U_2 \lesssim -0.2E_\mathrm{F}$.

We stress that in these qualitative arguments, evanescent waves have been ignored completely. In particular, for $U_2 \gtrsim -0.2E_\mathrm{F}$ (with other parameters fixed as given), both spin channels are evanescent in the central region ($0 < z < d$) and cannot be addressed within the approximate analytical method. (Even if the energy is positive, evanescent waves appear already for negative U_2 because of the strong Rashba SOC in the centeral region.) Quite interestingly, as we have seen above, the contributions of the evanescent waves are highly nontrivial in this parameter range and give rise to $-\cos(\phi/2)$ behavior.

6. Conclusion

We have considered a double-barrier MTJ consisting of a ferromagnetic electrode, a QW with magnetic ordering and strong Rashba spin–orbit coupling, and a normal metal electrode where the junction is formed on the cylindrical shell of the QW. The structure may have a relevance as a simplified model for the magnetic tunnel junction with a LAO/STO transition metal oxide interface including twin boundaries. The latter has been reported to exhibit sign-switching anisotropic TMR. By means of both qualitative analysis and numerically exact calculations, we have shown that our model exhibits a sign-switching anisotropic TMR. The negative TMR occurs as a combined effect of one-dimensionality, magnetic order, and strong SOC in the QW.

Acknowledgments

This work was supported by the BK21 Plus Project from the Korean Government and by MINECO (Spain) Grant FIS2011-23526.

References

[1] Wolf S A, Awschalom D D, Buhrman R A, Daughton J M, von Molnár S, Roukes M L, Chtchelkanova A Y and Treger D M 2001 *Science* **294** 1488
[2] Moodera J S, Miao G X and Santos T S 2010 *Phys. Today* **63** 46
[3] Miyazaki T and Tezuka N 1995 *J. Magn. Magn. Mater.* **139** L231
[4] Tsymbal E Y, Sokolov A, Sabirianov I F and Doudin B 2003 *Phys. Rev. Lett.* **90** 186602
[5] Sahoo S, Kontos T, Furer J, Hoffmann C, Gräber M, Cottet A and Schönenberger C 2005 *Nat. Phys.* **1** 99
[6] Cottet A, Kontos T, Sahoo S, Man H T, Choi M S, Belzig W, Bruder C, Morpurgo A and Schönenberger C 2006 *Semicond. Sci. Technol.* **21** S78
[7] Cottet A and Choi M S 2006 *Phys. Rev.* B **74** 235316
[8] Yuasa S, Nagahama T and Suzuki Y 2002 *Science* **297** 234
[9] Matos-Abiague A and Fabian J 2009 *Phys. Rev.* B **79** 155303
[10] Ngo T D N *et al* 2014 Polarity-tunable magnetic tunnel junctions based on ferromagnetism at oxide heterointerfaces unpublished

[11] Ohtomo A and Hwang H Y 2004 *Nature* **427** 423
[12] Reyren N *et al* 2007 *Science* **317** 1196
[13] Brinkman A, Huijben M, van Zalk M, Huijben J, Zeitler U, Maan J C, van der Wiel W G, Rijnders G, Blank D H A and Hilgenkamp H 2007 *Nat. Mater.* **6** 493
[14] Li L, Richter C, Mannhart J and Ashoori R C 2011 *Nat. Phys.* **7** 762
[15] Bert J A, Kalisky B, Bell C, Kim M, Hikita Y, Hwang H Y and Moler K A 2011 *Nat. Phys.* **7** 767
[16] Michaeli K, Potter A C and Lee P A 2012 *Phys. Rev. Lett.* **108** 117003
[17] Chen G and Balents L 2013 *Phys. Rev. Lett.* **110** 206401
[18] Kalisky B *et al* 2013 *Nat. Mater.* **12** 1091
[19] Ron A and Dagan Y 2014 *Phys. Rev. Lett.* **112** 136801
[20] Pentcheva R and Pickett W E 2009 *Phys. Rev. Lett.* **102** 107602
[21] Pentcheva R and Pickett W E 2007 *Phys. Rev. Lett.* **99** 016802
[22] Pentcheva R and Pickett W E 2008 *Phys. Rev.* B **78** 205106
[23] Gelabert M M and Serra L 2011 *Eur. Phys. J.* B **79** 341